AIAA SciTech Forum
11–15 & 19–21 January 2021, VIRTUAL EVENT
AIAA Scitech 2021 Forum

10.2514/6.2021-0844

Improved Fluid-Structure Interface for Aeroelastic Computations with Non-Matching Outer Mold Lines

Zhi Yang * and Dimitri J. Mavriplis †

A general three-dimensional algorithm for data transfer between fluid-structure meshes in aeroelastic computations is described in this paper. The algorithm is designed specifically for cases where the fluid and structural meshes exhibit significantly different outer mold lines, as is often the case when simplified structural models are used. The approach is based on the use of three-dimensional structural frame elements, which model the links created between the CFD surface mesh points and their projections on the structural mesh element surfaces. The algorithm can be used as an add-on to existing fluid-structure interfaces (FSI) which assume rigid links between the CFD surface points and the structural mesh in order to produce smoother displacement fields on the CFD surface mesh.The discrete adjoint of this FSI approach is also incorporated and the technique is demonstrated both on an analysis and a design optimization test case.

I. Introduction

Over the last decade, Reynolds-averaged Navier-Stokes (RANS) computational fluid dynamics (CFD) methods have become the high-fidelity analysis and design tool of choice in the aerospace industry for fixed and rotary wing aircraft. Although single discipline aerodynamic simulations are still most prevalent particularly for fixed wing applications, incorporating fully coupled aeroelastic effects is generally seen as the next step in the drive to higher fidelity analysis and optimization capabilities. Aeroelastic effects take on added importance for time-dependent problems such as fixed wing flutter problems and rotorcraft simulations, where the structural response and the coupling between fluid and structure plays a dominant role in the overall simulation.

Many aeroelastic simulation capabilities can be classified into two groups: one group that employs high fidelity aerodynamic models (ie. RANS) with simplified structural models (i.e. modal models), and a second group that employs high-fidelity finite element structural models along with simplified aerodynamic models. A modern high-fidelity aeroelastic capability must include both high-fidelity aerodynamic and structural models and these should be solved in a tightly coupled fashion for both steady-state and time-dependent problems.

In addition to the aeroelastic analysis problem, aeroelastic design optimization is increasingly being pursued as designers seek to incorporate higher-fidelity and additional disciplines at earlier stages of the design process. Since gradient-based optimization is generally taken to be the most viable approach at high fidelity, adjoint methods are necessary to obtain sensitivities of a single or small number of objectives with respect to large numbers of design parameters at reasonable cost. The use of adjoint equations is now fairly well established in steady-state aerodynamic shape optimization. Additionally, adjoint methods for coupled aeroelastic or aerostructural optimization have been pursued over the last decade by various contributors.[1–3]

In structural analysis, the body is often simplified by combinations of beam, brick, shell or other types of structural elements. In flow analysis, the solution requires an accurate description of the boundary. The computational nodes for the structure usually do not coincide with those used for the flow simulation. A key ingredient in those high-fidelity multidisciplinary analysis and optimization is the accurate data transfer between the CFD system and the computational structural dynamics (CSD) system.

The data transfer algorithm usually involves a combination of interpolation and extrapolation. Interpolation techniques such as the infinite or finite-plate spline methods and other spline interpolation methods

*Research Scientist, AIAA member; email: zyang@uwyo.edu
†Professor, AIAA Associate Fellow; email: mavriplis@uwyo.edu

work well as long as the structural grid points and the aerodynamic grid points are within the same surface. Harder and Desmarais[4] presented the surface spline interpolation also commonly known as infinite-plate spline (IPS) method. To obtain a smooth description of a transversely deformed plate supported on a finite number of known data, the equilibrium bending equations for an infinite plate are used. At least three non-collinear data points have to be used as support to define the planar distribution. The known data points do not have to be supported by a grid. Harder[4] presented a smoothing technique by applying distributed loads to improve the solution of the original method.

Pidaparti[5] proposed a method based on the inverse isoparametric mapping by first locating each point of interest within a structural element, then obtaining the local element coordinates of the interpolation point by numerically inverting the relationship between global and local coordinates applying nodal shape functions. The interpolation of data is performed by using the same shape functions. If the same shape functions are applied for interpolation and structural computation, this approach has the advantage of being consistent with the structural analysis.

Cebral and Lohner[6] proposed a method by treating each aerodynamic node as rigidly attached to the closest structural element for the case of a planar structural grid and a three-dimensional wing surface. The force transformation is conservative in the sense that the total force on the aerodynamic surface is the same as that on the structural grid. However, conservation of energy is not guaranteed. The equation is discretized by using a finite element grid and shape functions. A more general and often used approach based on rigid links can be found in various other references.[1,2]

Goura et al.[7] present a three-dimensional interpolation method for the problem of non-matching structural and aerodynamic surfaces. Each node on the CFD surface mesh is attached to a triangular structural element to form a tetrahedron. The orientation between the aerodynamic node and the structural element remains constant, while the distance is adjusted to obtain a Constant-Volume Tetrahedron (CVT). This method can exactly represent rigid body modes including rotation. The linearized CVT approach can be used for conservative displacement and force transformations.

Chen and Jadic[8] presented an approach based on physical considerations. Lai et al.[9] implemented this method for complex configurations by assuming a homogeneous elastic structure. A boundary element method can be applied to relate displacements of the aerodynamic boundary to displacements of internal structural nodes. By inverting this relation (using additional constraints such as minimum strain energy) the transformation matrix is obtained, which can be used to obtain a conservative interpolation scheme for the displacement transformation and the force transformation.

Samareh[10] presented a general three-dimensional algorithm for data transfer between dissimilar meshes. The method treats the structured and unstructured meshes in the same manner, can transfer scalar or vector fields between dissimilar surface meshes. The method is also applied in the integration of a scalar field on one mesh and injection of the resulting vectors onto another mesh.

Rendal[11] proposed a multivariate interpolation scheme by using radial basis functions. This method operated on totally arbitrary point clouds. All connectivity and user-input requirements are removed from the computational fluid dynamics/computational structural dynamics (CFD/CSD) coupling problem. Only point clouds are required to determine the coupling. This method can also be applied to structured and unstructured grids, or CSD and CFD grids that intersect, since no connectivity information is required.

In this paper, we present a simple data exchange algorithm, which is based on the three dimensional frame analogy, for high-fidelity CSD-CFD coupled solvers. The fomula for the algorithm will be presented in the next section, followed by a few selected cases to prove the efficiency and robustness of the algorithm.

II. Fluid-Structure Interface

In order to couple the computational structural dynamics (CSD) solver to the computational fluid dynamics (CFD) solver, a general fluid-structure interface (FSI) module has been developed. This interface is a stand-alone module that transfers the aerodynamic forces from the CFD solver to the CSD model, and also returns the displacements generated from the CSD solver to the CFD surface mesh. The FSI must be capable of handling non-point matched overlapping CFD and CSD surface meshes of widely varying resolution and element types. Additionally, the FSI must be capable of handling CSD models that do not match the outer-mold line (OML) of the geometry used for the CFD surface mesh. This situation can arise either due to small differences in the geometry representation used for the CFD and CSD model, or due to an incomplete CSD model, for example in cases where only a portion of the complete structure is used in the

CSD model, as is often the case in early design stages. In our original FSI implementation, which was based on rigid links, for each CFD surface point, the closest point on the surface of the CSD finite element mesh is found through a fast parallel search technique, which is based on the minimum distance search used for CFD turbulence model requirements. Once all CFD surface points have been associated with their closest perpendicular projection on the CSD surface mesh, the CFD forces and moments are transferred to the CSD surface nodes as:

$$F_{CSD} = [T]F_{CFD} \tag{1}$$

where [T] represents the rectangular transfer matrix which is computed assuming the surface CFD points are attached to their corresponding closest point on the surface CSD mesh via rigid links.[2,12] Conversely, the CSD displacements are transferred back to the CFD surface mesh as:

$$U_{CFD} = [T]^T F_{CSD} \tag{2}$$

By using the transpose of the force transfer matrix for the displacement transfer, the principle of conservation of virtual work is guaranteed. To enhance robustness and increase flexibility, all CFD surface points and CSD surface faces are associated with a component number and the user can specify which CFD components should transfer forces to which CSD components. In this manner, specific components that do not contribute to loads on the flexible structure can be omitted.

In our simulations, the above process can lead to non-smooth displacements interpolated on the CFD surface mesh due to the shape and location of the CSD surface mesh. In particular, for CFD surface mesh points that are a significant distance away from their closest projection on the CSD surface (which arises for large differences in the CFD and CSD outer mold lines) the rotations prescribed to the rigid links by the CSD displacement field result in amplification of the displacements on the CFD surface mesh points. Thus small irregularities in the CSD displacement field may show up as unphysical displacements on the CFD side. To cure this non-smooth interpolation, a simple data exchange algorithm, which is based on the three-dimensional flexible frame analogy, is presented, as shown in Figure 1.

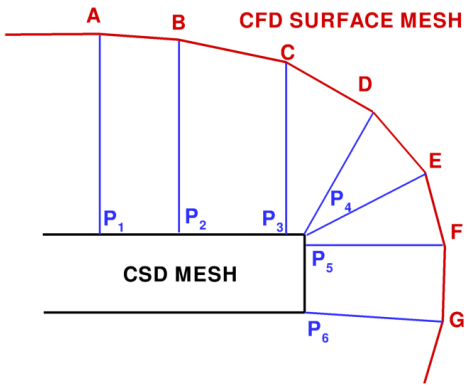

Figure 1. Illustration of the frame analogy.

The frame is constructed by the edges of the CFD surface mesh and the edges connecting the nodes on the CFD surface mesh to their projections on the CSD surface mesh. This construction is very straight forward because the projections of the CFD surface nodes on the CSD surface mesh are already obtained in the previously defined search process. Figure 2 shows the nodes of the three-dimensional frame, which consist of 2-node beam-rod elements, where E is the material modulus of elasticity, I is the cross-sectional moment of inertia, G is the modulus of elasticity in shear, J is the torsional constant of the cross section, and A is the cross-sectional area. The values of EA, EI and GJ for the frame elements can be adjusted to improve the smoothness of the final displacements. In general, two values are exposed to the user, one for the edges

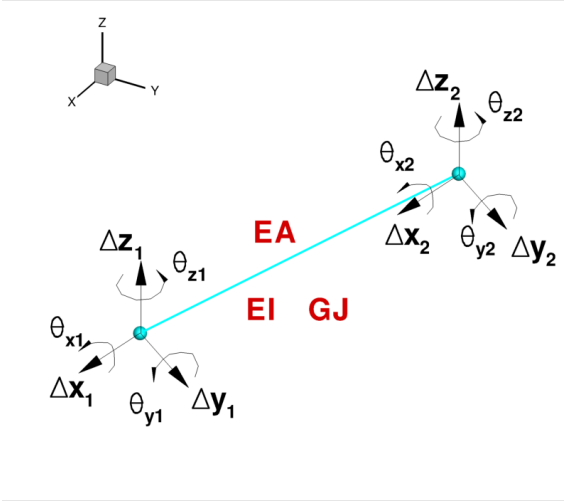

Figure 2. Node for the 3D rigid-jointed frame using 2-node beam-rod elements.

corresponding to the CFD surface mesh edges, and another for the values of the links joining the CFDF points to the CSD surface mesh. The equation and corresponding stiffness matrix for the beam element is:

$$EI\frac{d^4w}{dx^4} = q \tag{3}$$

where q is the transverse load, and

$$[K]_b^e = \frac{EI}{L^3}\begin{bmatrix} 12 & 6L & -12 & 6L \\ 6L & 4L^2 & -6L & 2L^2 \\ -12 & -6L & 12 & -6L \\ 6L & 2L^2 & -6L & 4L^2 \end{bmatrix} \tag{4}$$

The equation and corresponding stiffness matrix for the Rod element with axial displacement:

$$EA\frac{d^2u}{dx^2} + F = 0 \tag{5}$$

where F is the axial distributed load, and

$$[K]_r^e = \frac{EA}{L}\begin{bmatrix} 1 & -1 \\ -1 & 1 \end{bmatrix} \tag{6}$$

The equation and corresponding stiffness matrix for the Rod element with torsional displacement:

$$GJ\frac{d\theta}{dx} = T \tag{7}$$

where T is the torsional moment, and

$$[K]_t^e = \frac{GJ}{L}\begin{bmatrix} 1 & -1 \\ -1 & 1 \end{bmatrix} \tag{8}$$

The stiffness matrix of the frame is constructed by the superposition of the axial stiffness matrix Eq.(6), the beam stiffness matrix Eq.(4) and the torsional stiffness matrix Eq.(8).[13] The beam stiffness matrix is used twice in Y and Z direction. Then the stiffness matrix for the three dimensional frame element can be written

as:[13]

$$[K]^e = \begin{bmatrix} \frac{EA}{L} & & & & & & & & & & & \\ 0 & \frac{12EI_z}{L^3} & & & & & & & & & & \\ 0 & 0 & \frac{12EI_y}{L^3} & & & & & & & & & \\ 0 & 0 & 0 & \frac{GJ}{L} & & & & & & & & \\ 0 & 0 & -\frac{6EI_y}{L^2} & 0 & \frac{4EI_y}{l} & & & & & & & \\ 0 & \frac{6EI_z}{L^2} & 0 & 0 & 0 & \frac{4EI_z}{L} & & & & & & \\ -\frac{EA}{L} & 0 & 0 & 0 & 0 & 0 & \frac{EA}{L} & & & & & \\ 0 & -\frac{12EI_z}{L^3} & 0 & 0 & 0 & -\frac{EI_z}{L^2} & 0 & \frac{12EI_z}{L^3} & & & & \\ 0 & 0 & -\frac{12EI_y}{L^3} & 0 & \frac{6EI_y}{L^2} & 0 & 0 & 0 & \frac{12EI_y}{L^3} & & & \\ 0 & 0 & 0 & -\frac{GJ}{L} & 0 & 0 & 0 & 0 & 0 & \frac{GJ}{L} & & \\ 0 & 0 & -\frac{6EI_y}{L^2} & 0 & \frac{2EI_y}{l} & 0 & 0 & 0 & \frac{6EI_y}{L^2} & 0 & \frac{4EI_y}{L} & \\ 0 & \frac{6EI_z}{L^2} & 0 & 0 & 0 & \frac{2EI_z}{L} & 0 & -\frac{6EI_z}{L^2} & 0 & 0 & 0 & \frac{4EI_z}{L} \end{bmatrix} \quad Symmetric$$

We note that there are 12 degrees of freedom associated with each element, consisting of 3 displacements and 3 rotations at each of the two ends of the element. After assembling the stiffness matrix, we get the equation:

$$K\delta = \delta_p \tag{9}$$

where δ denotes the displacements and rotations at each node and δ_p are the displacements and rotations at the projection nodes. These values are prescribed from the displacement field of the structural model solution, and by solving the above equation, we obtain the displacements on the CFD surface mesh. The transpose of this process is used to produce moments and forces on the CSD surface mesh as a function of prescribed loads on the CFD surface mesh. To accelerate convergence of the linear system required for solution, a preconditioned GMRES solver is used. Figure 3 shows the convergence comparison using a point Jacobi iterative method as a solver and as a preconditioner for GMRES for a typical test case.

III. Results and Discussion

To demonstrate the performance of the frame-analogy method, several cases in which the interpolation method fails to produce a smooth CFD surface mesh are presented. Figure 4a shows outer mold line (OML) of a CFD mesh over the wing tip of the DLR F6 wing-body configuration. A notional structural model is also shown (in purple) which does not extend all the way to the wing tip and has slight differences in other regions with the CFD OML. Figure 4b shows the frames or links (orange line segments) which connect the CFD mesh points to the CSD surface mesh through the point projection algorithm. Figure 5 shows the comparison of the CFD surface mesh obtained by the rigid link interpolation method and the new frame algorithm after the CSD structural model undergoes a 15^o prescribed twist at the wing tip. The simpler interpolation approach results in non smooth displacements near the trailing edge due to the large discrepancy between the two outer mold lines near the wing tip, which results in jumps in the nearest point projection algorithm, as shown in Figure 5a. However, the CFD surface mesh produced by the frame algorithm using these same point projections is smooth, shown in Figure 5b.

A. Aerostructural Analysis of Slotted Natural Laminar Flow Configuration

In this section, the frame algorithm is used in an aerostructural analysis simulation which computes the flow over a notional SNLF aircraft configuration. This test case requires the coupled solution of the flow (RANS) equations, a suitable transition model, along with the structural model response. Figure 6 shows the structural finite element model of the wing-box in red visualized within the outer mold line of the CFD surface mesh for a Slotted Natural Laminar Flow (SNLF) configuration (grey). This case is particularly interesting since the wing box only spans a portion of the chord of the main element of the two element airfoil wing (fore element and flap). In practice, the flap is attached to the main wing box with structural connectors, although these are not present in the current structural model. Therefore, any bending and twisting of the wing box must be transferred to the flap element through the non-matching OML FSI. Note that the structural model also contains an external strut (not shown) which attaches to the fuselage for this

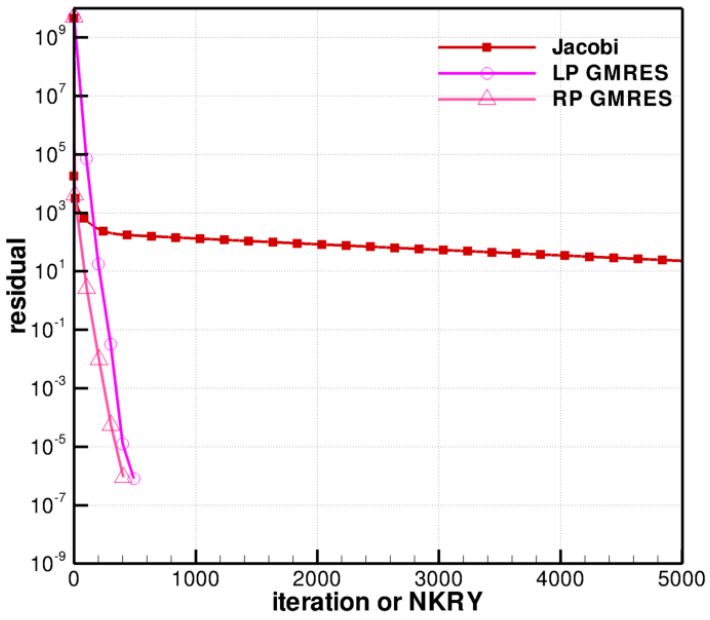

Figure 3. Convergence comparison between the Jacobi-iterative method(Jacobi), the left-precondition GMRES(LP GMRES) and the right-precondition GMRES(RP GMRES) method. Iteration for Jacobi, cumulative number of Krylov vectors (NKRY) for GMRES. Each symbol on GMRES lines represents one iteration.

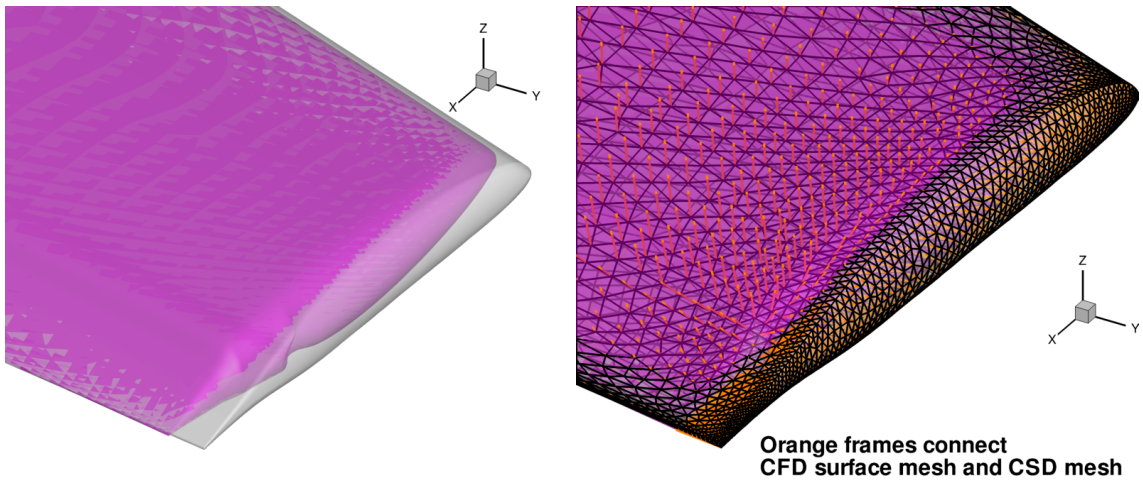

(a) (b)

Figure 4. (a): CSD(purple) and CFD surface(grey) for DLR F6 wing; (b): Line segments (orange) connecting the CFD mesh points to CSD surface mesh.

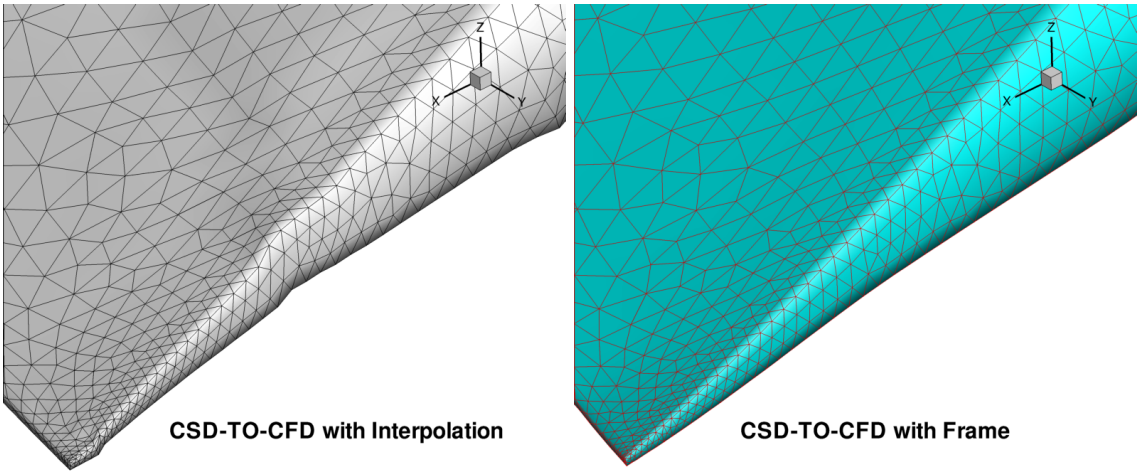

(a) (b)

Figure 5. CFD surface mesh obtained by using rigid link interpolation method (a), and the rigid-frame analogy (b).

truss-braced wing configuration. While the strut is present in the structural model, it is not modeled in the CFD mesh.

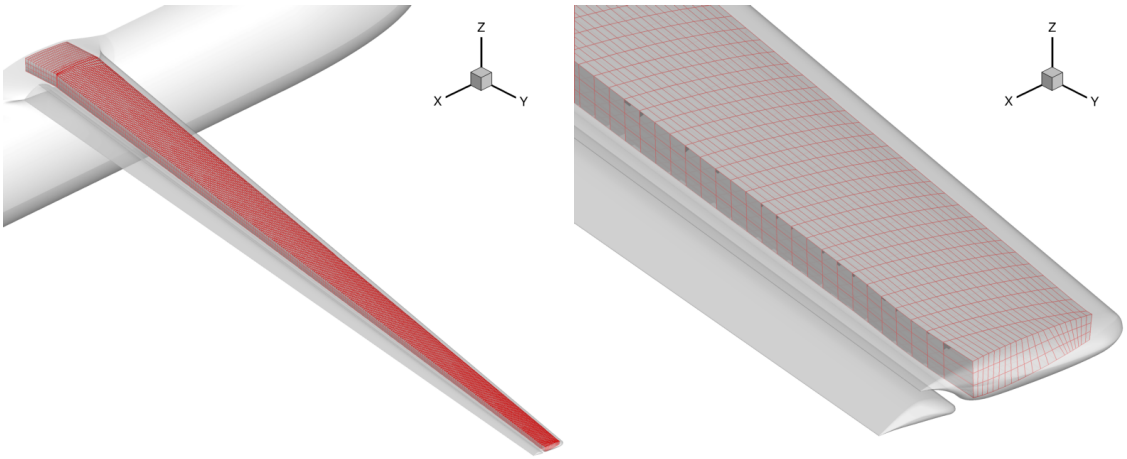

(a) (b)

Figure 6. (a) Structural finite element model of the wing-box visualized within outer mold line(red) and CFD surface(grey), (b) zoom in near the wing tip

To test the robustness of the aerostructural analysis system, we tested a range of cases with different prescribed wingbox twisting angles at specified spanwise stations. Figure 7 shows the wing tip CFD surface mesh for the Slotted Natural Laminar Flow(SNLF) configuration where a 5 degree twist angle is prescribed to the structural model which is then transferred to the CFD mesh. The CFD surface mesh produced by the interpolation method develops an irregularity on the flap upper surface, while the frame algorithm approach produces a smoothly displaced mesh. Figure 8 shows the same configuration but at higher twist angle(20 degree). The CFD surface mesh produced by the interpolation method shows a severe non-smooth dent, but the frame algorithm still produces a smooth CFD surface mesh.

A preliminary aero-structural analysis run is made in the absence of any transition model, using the

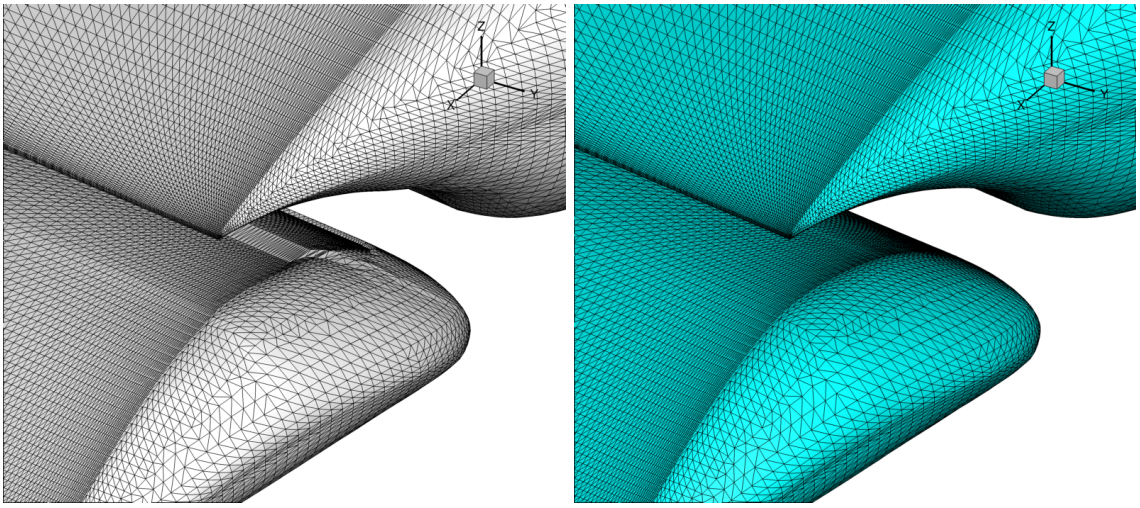

(a) (b)

Figure 7. The CFD surface mesh near tip: (a) interpolation, (b) rigid-frame analogy

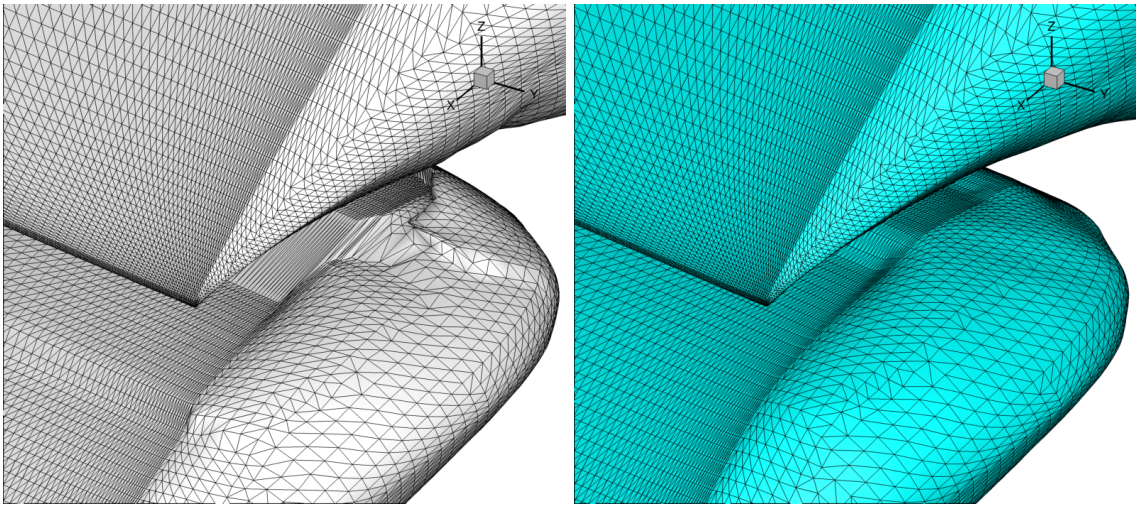

(a) (b)

Figure 8. The CFD surface mesh near tip: (a) interpolation, (b) rigid-frame analogy

Spalart Allmaras turbulence model. The flow conditions are taken as: $Ma = 0.5$, $\alpha = 1.7°$, $Re = 5 \times 10^6$. The convergence histories of the residual and the lift coefficient are shown in Figure 9. Figure 10 shows the pressure coefficient contours on the surface of the SNLF configuration. This case was run as a rigid wing (no structural model) and as a flexible wing with structural model, both fully turbulent and with free transition. Although a variety of transition models have been implemented and validated, the single equation model of Mentor[14] coupled with the single turbulence equation of Spalart-Allmaras(SA) was found to offer the most robust strategy for achieving consistent convergence to steady state. Results are illustrated in Figure 11, in terms of the wing tip deflection, showing the differences between rigid, aeroelastic and transitional effects on the computed wing tip deflection. The wing tip deflection for the fully turbulent aeroelastic case and the aeorelastic case with transition are 10.0 and 13.2 respectively, for a wing semi-span of 1020 units. The computed lift coefficients are given as 0.4998, 0.4839 and 0.3825 for the rigid transitional case, the flexible transitional case and the flexible fully turbulent case, respectively.

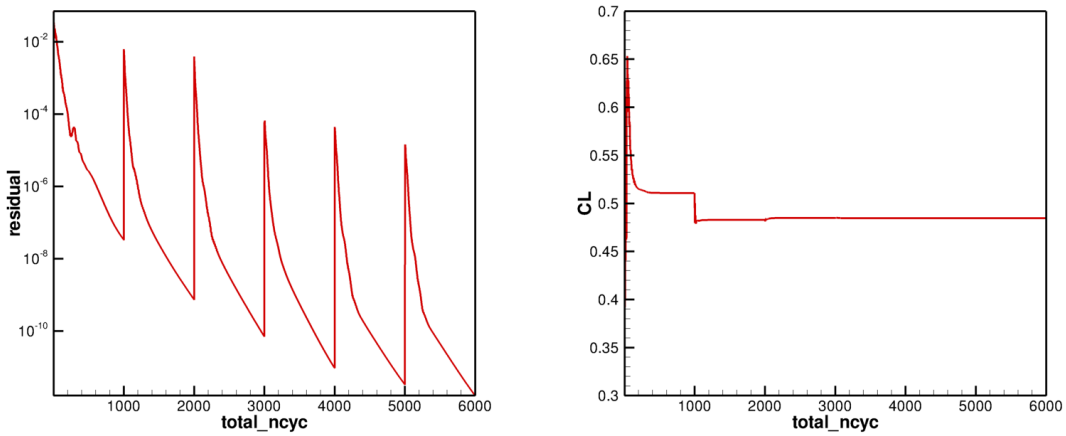

(a) (b)

Figure 9. Convergence history of flow residual(a) and the lift coefficient(b). Frame method.

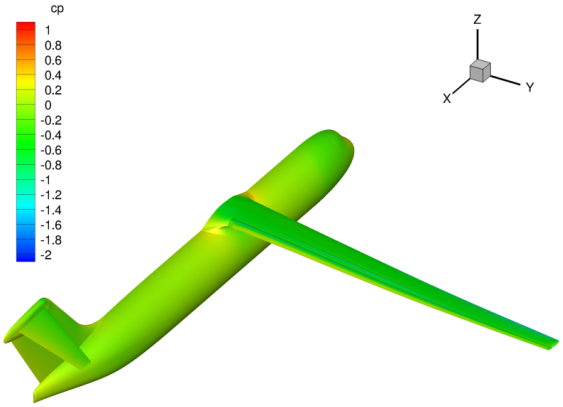

Figure 10. Pressure coefficient contours for aerostructural analysis with Frame method.

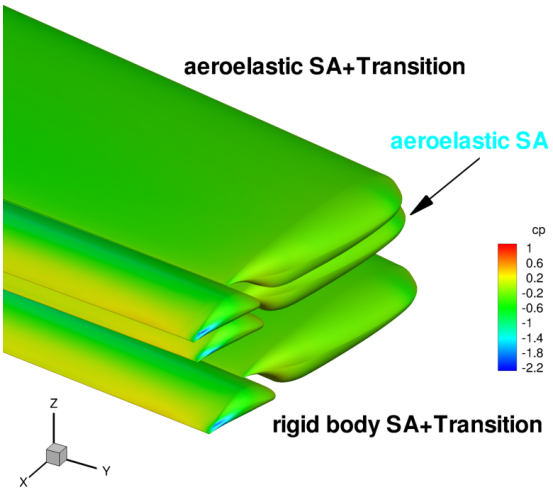

(a)

Figure 11. Comparison of wing tip deflections

B. Aerostructural Optimization of Slotted Natural Laminar Flow Configuration

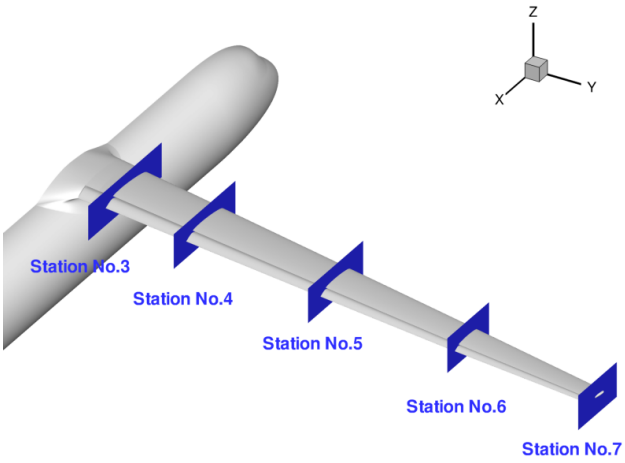

Figure 12. Illustration of spanwise stations for wing twist design variables.

One of the principal objectives of this work is the development of a design optimization capability for SNLF aircraft configurations. To this end, a discrete adjoint formulation for computing sensitivities has been incorporated into all of the individual disciplinary components of the current analysis capability. For the RANS CFD solver, this includes the discrete adjoint of the transition model. The adjoint of the new frame-element based FSI interface has also been implemented and coupled to the CFD and CSD disciplinary adjoint formulations. In previous work, we have shown the verification and demonstration of the adjoint-based optimization capability for natural laminar flow configurations in the absence of structural effects (i.e. rigid model). In this paper, aerostructural optimization of the SNLF configuration is demonstrated using the discrete adjoint of the coupled aero-structural analysis capability including the frame-based fluid-structure interface. For this purpose we employ the notional SNLF aircraft configuration described previously with

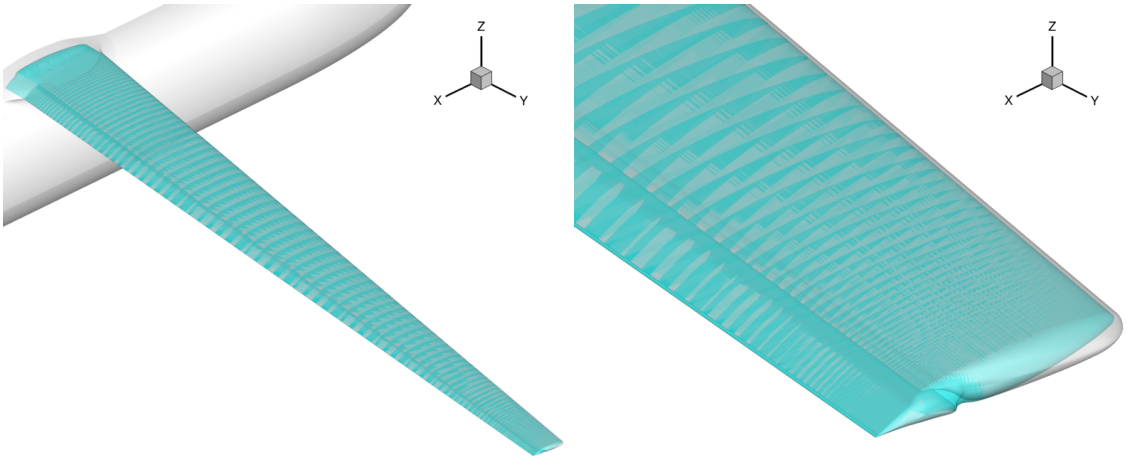

(a) (b)

Figure 13. (a) Geometry model(teal) and CFD surface(grey), (b) zoom in near the wing tip

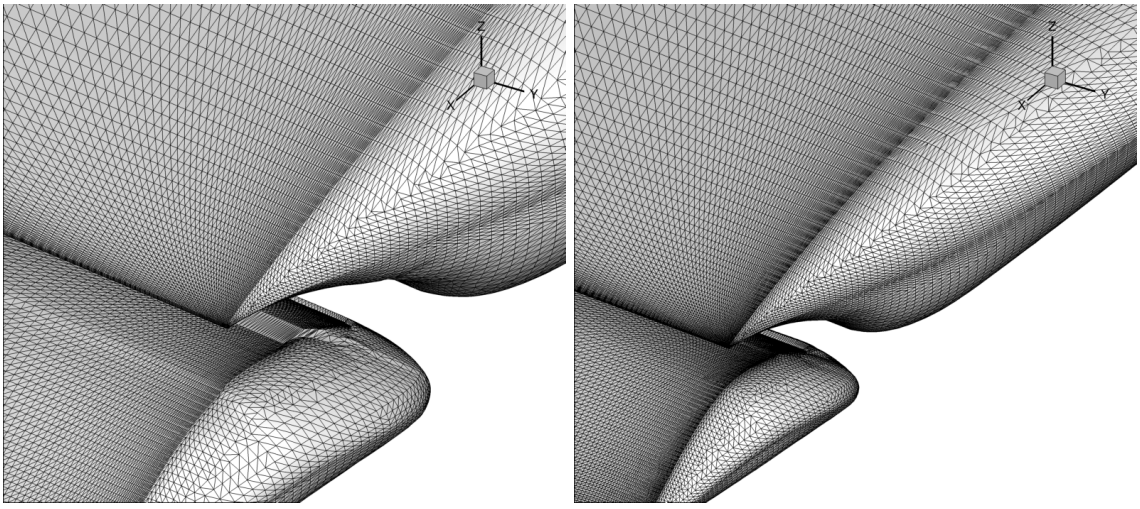

(a) (b)

Figure 14. (a) Non-smooth CFD surface mesh due to design shape change (b) smooth CFD surface mesh using frame analogy for same design shape change.

five design parameters defining wing twist at spanwise stations as shown in Figure 12.

Our optimization shape design variable module relies on a lofting process, where a wing jig shape is built up based on a series of sectional airfoils along with twist, taper, sweep and other parameters. The wing jig shape approximates the shape of the initial CFD surface mesh and surface displacements on the jig shape resulting from design changes are transferred to the CFD surface mesh using either the rigid link interpolation approach or the new frame-element method. For this case, the wing airfoil cross-sectional shapes are to be held fixed, and in order to apply global shape changes such as twist and taper to both main and flap elements, we employ a single element cross sectional airfoil which approximates the shape of the combined two-airfoil system (in the absence of a slot). The constructed jig shape is shown in Figure 13 where it is overlaid with the CFD surface mesh. Here again, the rigid link FSI approach produces a non-smooth surface CFD mesh when the wing tip is twisted in response to the input shape design variables, while the frame-based FSI approach produces smooth changes as shown in Figure 14. In the following optimization test case, the

frame-based FSI approach is used for both the transfer of shape design changes and structural deflections to the surface CFD mesh, and the discrete adjoint of this process is coupled to the other disciplinary adjoints and used in the sensitivity analysis phase.

An important consideration for the successful computation of sensitivities using the discrete adjoint approach is the ability to fully converge the primal equations prior to solving the adjoint system. As mentioned previously, the presence of the coupled transition equation(s) can significantly impair the ability of the solver to reach low residual or tolerance levels in convergence to steady state. In the current work, although a variety of transition models have been implemented and validated, the single equation model of Mentor[14] coupled with the single turbulence equation of Spalart-Allmaras was found to offer the most robust strategy for achieving consistent convergence to steady state. However, even with this model, localized jumps in the intermittency values in the sublayer region may be observed which can stall convergence. Therefore, a strategy of freezing the intermittency values after a period of initial convergence during which the aerodynamic force coefficients achieve near constant values was adopted. Figure 15 illustrates the solution process for flow over the SNLF aircraft configuration at $Mach = 0.5$, $Re = 5 \times 10^6$ and an incidence of 1.76°. The convergence of the flow, turbulence and transition (intermittency) equations is shown in Figure 15(a), with the corresponding convergence in force coefficients given in Figure 15(b). As can be seen, convergence of the intermittency equations stalls out after approximately 500 cycles, which eventually leads to a slowdown or stalling of the turbulence and flow equations. However, the force coefficients achieve near constant values within this period of the convergence history. Therefore, the intermittency field is frozen after 800 cycles, after which convergence of the flow and turbulence equations resumes as the corresponding residuals are driven to machine zero over several thousand additional cycles.

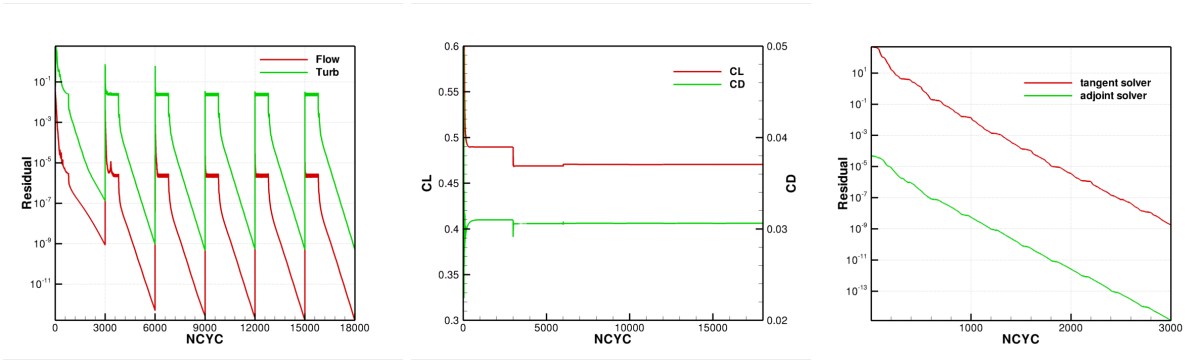

(a) (b) (c)

Figure 15. (a)Convergence history of flow, turbulence and transition(intermittency) equations;(b) Convergence history of computed force coefficients for initial configuration used in design optimization study; (c) Convergence history of tangent and adjoint solvers for computing sensitivities showing monotone convergence and similar convergence rates for both formulations.

Figure 15(c) depicts the convergence of the coupled system of discrete adjoint equations for the combined flow-turbulence-transition system linearized about the final state of the fully converged primal equations. The convergence of the tangent or forward linearization system is also shown. In both cases, the equations are solved using a restarted GMRES approach with line-implicit linear multigrid preconditioning, and monotone convergence to machine zero tolerance levels is observed with similar asymptotic convergence rates. Here the tangent system is used only for verification purposes and the similar convergence rates provide additional evidence that the adjoint system is solved appropriately, since theoretically these two linear problems contain the same eigenvalues and should converge at the same asymptotic rate.

In order to demonstrate the optimization process for flows with natural laminar transition, we construct a single objective function of the form:

$$L = (C_L - C_{L_{Target}})^2 + 10(C_D - C_{D_{Target}})^2 \tag{10}$$

The adjoint-based sensitivities for this objective function with respect to the five wing twist design variables are computed at each design cycle and supplied to the SNOPT optimizer[15] which controls the overall optimization process. This objective formulation can be used to minimize drag at a prescribed or fixed

lift condition. For these purposes, a target C_L value of 0.47 was chosen and the value $C_{D_{Target}} = 0.0$ was used to minimize drag in the optimization process. Although SNOPT is capable of performing constrained optimization, the above penalty-based objective formulation is used for simplicity at this stage.

For the initial configuration, we purposely apply an initial twist distribution that produces turbulent flow over a significant portion of the wing span, in order to investigate if the optimizer can find the low drag laminar flow solution. Figure 16(a) and (b) shows the optimization history of the objective and force coefficients over 38 design cycles. In this case the initial C_L and C_D values were 0.470 and 0.0306 respectively and and the optimization process resulted C_L and C_D values of 0.467 and 0.0262 respectively, corresponding to a drag reduction of 44 counts (at slightly lower lift). Figure 17 shows the computed skin friction coefficient on the initial and final optimized configuration, showing how the large regions of turbulent flow on the wing in the initial configuration have been replaced by laminar flow in the optimized configuration. The optimized wing twist includes approximately 0.5^o of negative twist at the wing tip, presumably in an effort to reduce induced drag.

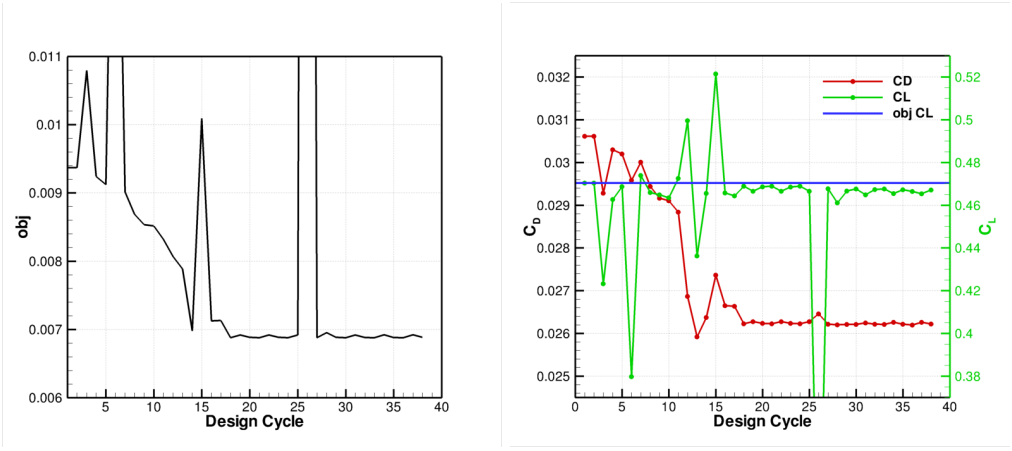

(a) (b)

Figure 16. (a) Convergence history for the objective function and (b) for integrated force coefficients CL and CD as a function of design cycles throughout the optimization process with CSD.

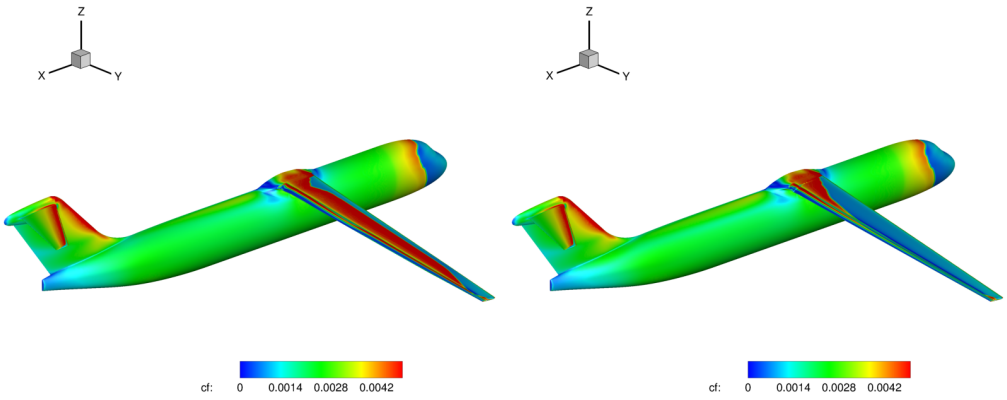

(a) (b)

Figure 17. Computed skin friction distribution for initial configuration(a) and optimized configuration(b) for wing twist optimization run.

IV. Conclusions

This paper describes an approach for improving the robustness of fluid structure interfaces for cases where the outer mold lines of the CFD and CSD meshes are substantially different. The method can be thought of as a smoothing technique for the displacements and rotations transmitted from the structural analysis components to the CFD surface mesh. However, the approach is based on a physical analogue which approximates to some degree the usual missing components such as structural skin elements by modeling the CFD surface mesh as an elastic component based on frame elements. The methodology is verified through several test cases. The results of those cases demonstrate the robustness of the algorithm, compared to the rigid link interpolation method. The aerostructural optimization of an SNLF configuration with free transition was also demonstrated using the discrete adjoint of the coupled aero-structural analysis capability including the frame-based fluid-structure interface.

References

[1]J. Reuther, J. J. Alonso, Joaquim R. R. A. Martins, and S. C. Smith. A coupled aero-structural optimization method for complete aircraft configurations. In *Proceedings of the 37th AIAA Aerospace Sciences Meeting and Exhibit*, Reno, NV, January 1999. AIAA 99-0187.

[2]Graeme J. Kennedy and Joaquim R. R. A. Martins. A parallel aerostructural optimization framework for aircraft design studies. *Structural and Multidisciplinary Optimization*, 50(6):1079–1101, December 2014.

[3]D. J. Mavriplis M. Asitav, M. Karthik and J. Sitaraman. Time-dependent adjoint-based aerodynamic optimization for coupled fluid-structure problems. *Journal of Computational Physics*, 292, 2015.

[4]R. L. Harder and R. N. Desmarais. Interpolation using surface splines. *Journal of Aircraft*, 9:189–191, 1972.

[5]R. M. V. Pidaparti. Structural and aerodynamic data transformation using inverse isoparametric mapping. *Journal of Aircraft*, 29:507–509, 1992.

[6]J. J. Cebral and R. Lohner. Conservative load projection and tracking for fluid-structure problems. *AIAA Journal*, 35:687–692, 1997.

[7]G. S. L. Goura, K. J. Badcock, M. A. Woodgate, and B. E. Richards. Transformation methods for the time marching analysis of flutter. AIAA Paper 2001-2457, 2001.

[8]P. C. Chen and I. Jadic. Interfacing of fluid and structural models via innovative structural boundary element method. *AIAA Journal*, 36:282–287, 1998.

[9]K. L. Lai, H. M. Tsai, and K. Y. Lum. A cfd and csd interaction algorithm for large and complex configurations. AIAA Paper 2002-2715, 2002.

[10]J. A. Samareh. Discrete data transfer technique for fluid-structure interaction. AIAA Paper 2007-4309, 2007.

[11]T. C. S. Rendal and C. B. Allen. Unified fluid–structure interpolation and mesh motion using radial basis functions. *International Journal for Numerical Methods in Engineering*, 74:1519–1559, 2008.

[12]Guru P. Guruswamy. A review of numerical fluids/structures interface methods for computations using high-fidelity equations. *Computers and Structures*, 80:31–41, 2002.

[13]Mario Paz and Young Hoon Kim. *Structural Dynamics: Theory and Computation*. Springer International Publishing, sixth edition, 2018.

[14]F. R. Menter, P. E. Smirnov, T. Liu, and R. Avancha. A one-equation local correlation-based transition model. *Flow, Turbulence and Combustion*, 95(4):583–619, 2015.

[15]P. E. Gill, W. Murray, and M. A. Saunders. SNOPT: An SQP algorithm for large-scale constrained optimization. *SIAM journal on optimization*, 12(4):979–1006, 2002.